THYROID
Volume 31, Number 8, 2021

DOI: 10.1089/thy.2020.0931

The Iodide Transport Defect-Causing Y348D Mutation in the Na^+/I^- Symporter Renders the Protein Intrinsically Inactive and Impairs Its Targeting to the Plasma Membrane

Andrea Reyna-Neyra,[1,*,§] Lara Jung,[1,†,§] Mayukh Chakrabarti,[2] Mikel X. Suárez,[1,‡] L. Mario Amzel,[2] and Nancy Carrasco[1,*,i]

Background: The sodium/iodide (Na^+/I^-) symporter (NIS) mediates active transport of I^- into the thyroid gland. Mutations in the *SLC5A5* gene, which encodes NIS, cause I^- transport defects (ITDs)—which, if left untreated, lead to congenital hypothyroidism and consequent cognitive and developmental deficiencies. The ITD-causing NIS mutation Y348D, located in transmembrane segment (TMS) 9, was reported in three Sudanese patients.
Methods: We generated cDNAs coding for Y348D NIS and mutants with other hydrophilic and hydrophobic amino acid substitutions at position 348 and transfected them into cells. The activity of the resulting mutants was quantitated by radioiodide transport assays. NIS glycosylation was investigated by Western blotting after endoglycosidase H (Endo H) and PNGase-F glycosidase treatment. Subcellular localization of the mutant proteins was ascertained by flow cytometry analysis, cell surface biotinylation, and immunofluorescence. The intrinsic activity of Y348D was studied by measuring radioiodide transport in membrane vesicles prepared from Y348D-NIS-expressing cells. Our NIS homology models and molecular dynamics simulations were used to identify residues that interact with Y348 and investigate possible interactions between Y348 and the membrane. The sequences of several Slc5 family transporters were aligned, and a phylogenetic tree was generated in ClustalX.
Results: Cells expressing Y348D NIS transport no I^-. Furthermore, Y348D NIS is only partially glycosylated, is retained intracellularly, and is intrinsically inactive. Hydrophilic residues other than Asp at position 348 also yield NIS proteins that fail to be targeted to the plasma membrane (PM), whereas hydrophobic residues at this position, which we show do not interact with the membrane, rescue PM targeting and function.
Conclusions: Y348D NIS does not reach the PM and is intrinsically inactive. Hydrophobic amino acid substitutions at position 348, however, preserve NIS activity. Our findings are consistent with our homology model's prediction that Y348 should face the side opposite the TMS9 residues that coordinate Na^+ and participate in Na^+ transport, and with the notion that Y348 interacts only with hydrophobic residues. Hydrophilic or charged residues at position 348 have deleterious effects on NIS PM targeting and activity, whereas a hydrophobic residue at this position rescues NIS activity.

Keywords: sodium/iodide symporter, iodide transport defect-causing NIS mutations, Y348D NIS, intracellular retention of NIS, molecular dynamics simulations

Introduction

Iodine is an essential constituent of the thyroid hormones (THs), which are not only crucial for the early development and maturation of the central nervous system, skeletal muscle, and lungs but are also master regulators of intermediary metabolism. Iodide (I^-) is scarce in the environment, and an insufficient dietary supply of I^- remains a major health problem worldwide (1,2).

The sodium/iodide (Na^+/I^-) symporter (NIS) is the key plasma membrane (PM) glycoprotein that mediates the active transport of I^- from the bloodstream into the thyroid gland,

[1]Department of Molecular Physiology and Biophysics, Vanderbilt University School of Medicine, Nashville, Tennessee, USA.
[2]Department of Biophysics and Biophysical Chemistry, Johns Hopkins University School of Medicine, Baltimore, Maryland, USA.
**Current address:* Department of Molecular Physiology and Biophysics, Vanderbilt University School of Medicine, Nashville, Tennessee, USA.
[†]*Current address:* Heidelberg University School of Medicine, Heidelberg, Germany.
[‡]*Current address:* University College London Medical School, London, United Kingdom.
[§]These authors contributed equally to this work.
[i]ORCID ID (https://orcid.org/0000-0001-8586-6249).

the first step in the biosynthesis of the THs (3–5). NIS-mediated I^- transport is electrogenic: 2 Na^+ ions are translocated per I^- ion (6). A remarkable property of NIS is that although its K_M for I^- transport is 5–10 μM, it transports I^- efficiently, even though the extracellular concentration of I^- is in the sub-μM range. This is because, at the physiological Na^+ concentration, more than 79% of the NIS molecules have 2 Na^+ ions bound to them, so NIS is poised to co-transport I^- (7). NIS is the molecule at the center of the treatment for thyroid cancer based on radioiodide administered after thyroidectomy, the most effective internal radiation cancer treatment available (8).

To date, 19 mutations in the gene that encodes NIS (*SLC5A5*) have been identified in patients (8–11). These mutations cause I^- transport defects (ITDs), which, if not detected and treated immediately after birth, can lead to congenital hypothyroidism (CH), goiter, stunted development, and cognitive impairment (10,12–16).

NIS has 13 transmembrane segments (TMSs), with an extracellular amino terminus and intracellular carboxy terminus (Fig. 1A) (5,17). The molecular characterization of NIS mutant proteins found in patients has yielded a wealth of mechanistic information about the transporter (8,16–26).

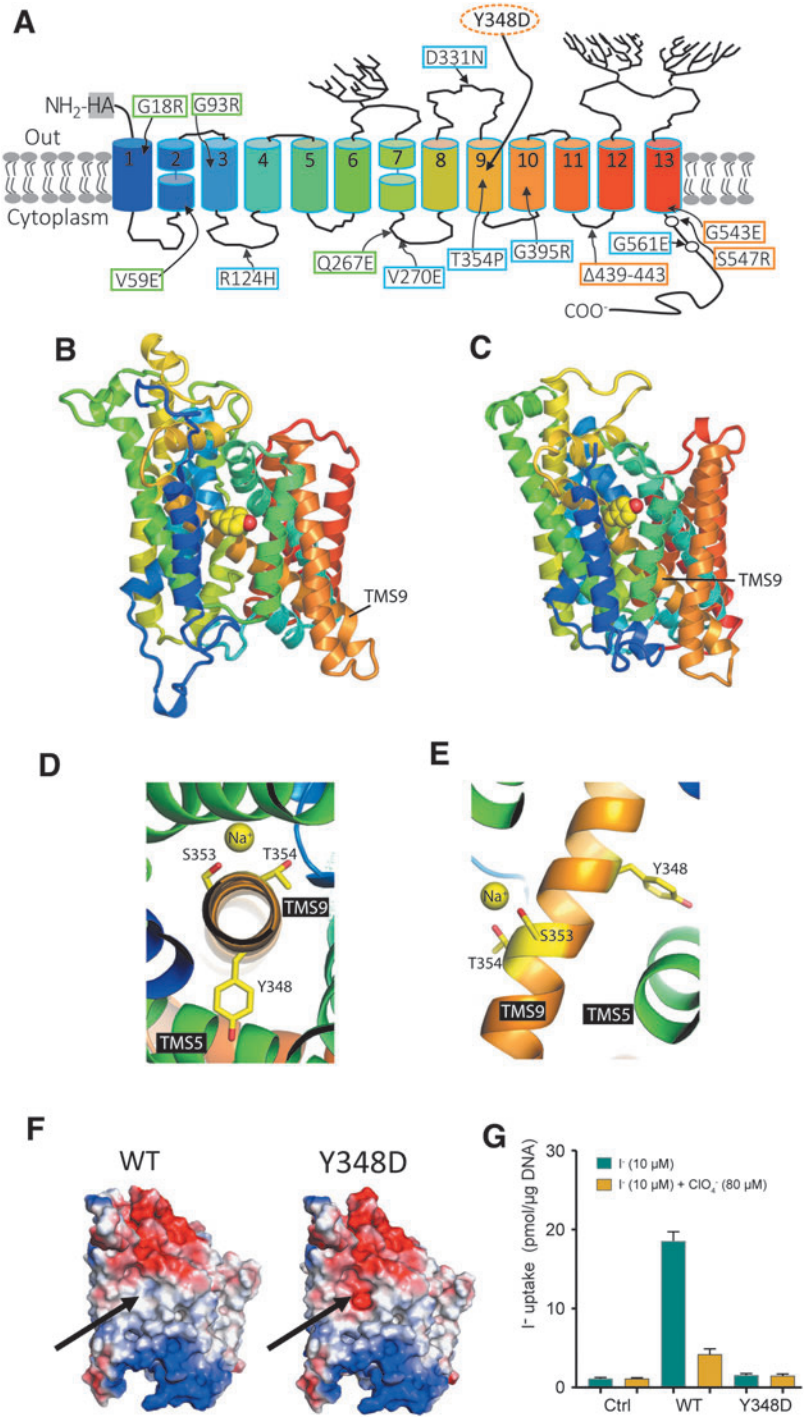

FIG. 1. The Y348D amino acid substitution, which is in TMS9, yields a NIS protein that does not transport I^-. (**A**) Experimentally tested secondary structure model of NIS showing 13 TMSs (colored cylinders) and 3 glycosylation sites (branches). ITD-causing NIS mutations, including Y348D, are shown next to the affected positions. Mutations that yield proteins that are both intrinsically inactive and retained intracellularly are shown in orange rectangles, nonfunctional proteins in green rectangles, and intrinsically active but intracellularly retained proteins in blue rectangles. An extracellularly facing HA tag was engineered at the N-terminus. (**B**) NIS homology model [cf. (23)] (inwardly open conformation). (**C**) New NIS homology model (*outwardly* open conformation), generated using as a template the Na^+-coupled sialic acid symporter, which has 25% sequence identity and 46% sequence similarity to NIS. The location of the Y348 residue (yellow) in TMS9 (orange) is shown in both **B** and **C**. (**D, E**) Y348 is on the side in TMS9 opposite that of S353 and T354, which coordinate Na^+ (21). (**F**) Electrostatic surface of WT and Y348D NIS. Positive and negative potentials are shown in blue and red, respectively, and the position of Y348 is indicated by a black arrow. (**G**) Steady-state I^- transport assay (30 min) in MDCK II cells transfected with control (pcDNA3.1), human WT, or Y348D NIS HA-cDNA in the presence or absence of ClO_4^- (gray bars) at 10 μM I^-/140 mM Na^+. ClO_4^-, perchlorate; HA, hemagglutinin; I^-, iodide; ITD, I^- transport defect; MDCK-II, Madin-Darby canine kidney; NIS, sodium/iodide symporter; TMSs, transmembrane segments; WT, wild type.

Watanabe *et al.* (10) identified, in three siblings, a homozygous missense mutation in the *SLC5A5* gene that causes a Tyr-to-Asp substitution at position 348 of NIS. The younger siblings were diagnosed with CH at 8 and 22 days of age and developed properly owing to levothyroxine treatment. However, the oldest sibling was diagnosed at 40 days of age and developed a cognitive deficit because she was treated too late (10). These authors noted that the mutation is located in TMS9 of NIS (Fig. 1A), which contains several amino acid residues important for Na^+ binding and/or translocation (21,27).

In this study, we investigate the effects of the Y348D mutation on NIS subcellular localization and function. Our findings demonstrate that Y348D NIS is both retained intracellularly and intrinsically inactive. Y348 does not face the Na^+ translocation pathway but rather is located on the other side of the helix and is surrounded mostly by hydrophobic residues. In the context of the evolutionary conservation of the residue at position 348 in the SLC5A5 family, we suggest that a hydrophobic residue is needed at that position to satisfy structural and functional requirements.

Materials and Methods

Site-directed mutagenesis, cell culture transfection and transduction, I^- uptake in whole cells and in membrane vesicles (MVs), flow cytometry, cell surface biotinylation, immunofluorescence, deglycosylation assays, and immunoblot were carried out as described previously (16,20,23).

NIS homology models

Our homology model of NIS in the *inwardly* open conformation (23) was based on the bacterial Na^+/galactose transporter (vSGLT) (PDB ID: 3DH4, 2XQ2; identity 27% and similarity 45%) (28,29). Our model of NIS in the *outwardly* open conformation (residues 11–550; the last extracellular loop was shortened by 40 residues) was generated using as a template the Na^+-coupled sialic acid symporter SiaT (PDB ID: 5NVA; 25% identity and 46% similarity to NIS) (30). Modeling was carried out with Modeller and the SwissProt server. The initial models were carefully analyzed, and insertions and deletions in helices were corrected; in addition, the hydropathy of aligned residues was matched. After several rounds of corrections, the inwardly and outwardly open models were aligned to ensure that the helices in the two structures aligned correctly. Clashes were removed by energy minimization using Gromacs (31,32). Residues with side chain non-hydrogen atoms 5 Å or less from the Y348 side chain were identified using PyMOL and an in-house Python script (as described in Computational studies).

Computational studies

All-atom isothermal-isobaric simulations of inwardly and outwardly open NIS were run with the CHARMM 36 forcefield (33) at 310 K using periodic boundary conditions and Ewald summation. The time step was 2-fs recording frames every 20 ps. A Langevin thermostat was used to heat the systems. The protein was solvated with the TIP3P water model and packed into a central 1-palmitoyl-oleoyl-sn-glycerol-phosphocholine (POPC) using the CHARMM-GUI web server (34–36). To prevent ion gradients established across the NIS-containing membrane from being dissipated by the periodic boundary conditions, a 1,2-dilauroyl-sn-glycero-3-phosphocholine (DLPC) bilayer was manually added to the system. Two sodium ions, as well as the I^- NIS ligands, were placed at the positions we determined previously. The three ions were positionally restrained with a force constant of 2.4 kcal/mol/Å^2. The inwardly and outwardly open NIS conformations were equilibrated in six steps before the production molecular dynamics (MD) runs. An in-house Python script was used to find residues that contact Y348 in the MD simulations. This script identifies as a contact in a frame a residue containing a side chain non-hydrogen atom 5 Å or less from the side chain atoms of Y348.

All frames from the simulation were used in the contact analysis (20,001 frames for the inwardly open conformation and 25,001 frames for the outwardly open conformation). The frequencies for this analysis were computed as the fraction of all frames in which the contact was present. In the cases in which multiple side chain non-hydrogen atoms in a residue were 5 Å or less from the side chain atoms of Y348, the highest frequency interaction was reported.

Sequence analysis

Representative SLC5 sequences were obtained by the BLAST search and aligned with ClustalX. A phylogenetic tree was inferred using the neighbor-joining method using only positions without gaps and with corrections for multiple substitutions, also in ClustalX. The drawing of the tree was facilitated by dendrogram.

Results

Cells transfected with Y348D NIS cDNA exhibit no I^- transport activity

Y348 is located in the middle of TMS9 (Fig. 1A–F). Our homology models of NIS in the inwardly (23) and outwardly open orientations predict that Y348 should face the side of the helix opposite S353 and T354 (Fig. 1D–E), residues that are key for the binding of Na^+ to the Na2 binding site (21,27). This suggests that the effect of the Y348D substitution is not related to Na^+ binding or translocation (21). To elucidate the effect of the Y348D substitution on NIS, we transfected wild-type (WT) or Y348D NIS cDNAs into Madin-Darby canine kidney (MDCK-II) cells and assayed them for I^- transport in the presence and absence of perchlorate (ClO_4^-), a competitive NIS inhibitor that is also transported by NIS (37) (Fig. 1G).

Consistent with the observations from the patients carrying the Y348D NIS mutant protein (10), the cells expressing Y348D NIS transported no I^-, even when the assay was carried out at 100 μM I^- (Supplementary Fig. S1), a concentration 10 times the K_M of human NIS (hNIS) for I^- (16).

Y348 is found in an uncharged hydrophobic region of NIS (as shown by the electrostatic surface; Fig. 1F). Thus, a charged residue at this position—such as Asp in Y348D NIS—probably destabilizes the interaction between TMS9 and the neighboring NIS helices, preventing the protein from being correctly assembled and properly inserted into the membrane.

Y348D NIS is retained intracellularly

NIS is glycosylated at Asn residues at positions 225, 489, and 502 (Fig. 1A). We carried out immunoblot analyses of membrane protein fractions from MDCK-II cells transfected with WT or Y348D NIS cDNA using our high-affinity

antibody against the carboxy terminus of hNIS (16,38). As expected, WT NIS was detected as a mature ~75–100 kDa polypeptide. Strikingly, however, no mature ~75–100 kDa Y348D NIS polypeptide was detected (Fig. 2A), even when the amount of protein electrophoresed was five times the amount of WT NIS. The partially glycosylated WT NIS and Y348D NIS polypeptides (~60 kDa) were readily apparent. NIS-mutant proteins that are not fully glycosylated oligomerize (20,26). This oligomeric species (~120 kDa) was also observed not only with Y348D NIS but also with NIS mutants with other amino acid substitutions at position 348 that prevent the proteins from being fully glycosylated.

Endoglycosidase H (Endo H) does cleave Asn-linked hybrid and high-mannose oligosaccharides, but not complex oligosaccharides, which are added to glycoproteins in the *trans*-Golgi. Endo H treatment of the membrane fraction shifted the partially glycosylated WT NIS from 60 kDa down to the ~50 kDa non-glycosylated form—but there was no effect on the mature ~75–100 kDa protein, in agreement with previous findings (16,20,24,26). Endo H treatment similarly shifted the immature core-glycosylated 60 kDa Y348D NIS and its dimer to its non-glycosylated ~50 and ~100 kDa forms (Fig. 2A). PNGase F is an amidase that cleaves between the innermost *N*-acetylglucosamine and Asn residues of high-mannose, hybrid, and complex oligosaccharides.

PNGase F treatment of the membrane fraction shifted both the mature ~75–100 kDa and the partially glycosylated 60 kDa WT NIS polypeptide, as well as the partially glycosylated ~60 kDa Y348D NIS polypeptide, down to their ~50 kDa non-glycosylated forms (Fig. 2B). These findings indicate that Y348D NIS is core-glycosylated, yielding a partially glycosylated polypeptide similar to its WT NIS counterpart, but Y348D NIS undergoes no further glycosylation in the *trans*-Golgi and therefore does not mature completely. Although we have reported that glycosylation is *not* required for WT NIS to be properly targeted to the PM and fully functional (5,24), most ITD-causing NIS mutants that are not properly targeted to the PM are not fully glycosylated (20,24,26). Therefore, we investigated the subcellular localization of Y348D NIS.

We carried out flow cytometry (FC) analyses of nonpermeabilized and permeabilized WT or Y348D NIS-expressing MDCK-II cells, using an anti-hemagglutinin (HA) antibody directed against an HA tag engineered onto the amino-terminus of NIS (Fig. 1A). Although the total expression of Y348D NIS was indistinguishable from that of WT NIS (Fig. 2C, left panel), the expression of Y348D NIS at the PM was negligible, in contrast to that of WT NIS (Fig. 2C, right panel). Cell surface biotinylation experiments were also performed with the membrane-impermeant compound sulfo-NHS-SS-biotin. An ~100 kDa polypeptide corresponding to mature WT NIS was observed in WT NIS-expressing cells, but not in Y348D NIS-expressing cells (Fig. 2D), providing further evidence that Y348D NIS does not reach the cell surface.

This conclusion was also supported by our immunofluorescence results. Using an anti-HA antibody, we investigated the subcellular localization of WT and Y348D NIS in MDCK-II cells. Under nonpermeabilized conditions, which reveal only proteins at the PM, WT NIS was readily apparent, but Y348D NIS was not (Fig. 2E). Under permeabilized conditions, Y348D NIS was clearly located exclusively inside the cell. In addition, Y348D NIS colocalized with the GM-130 protein, a *cis*-Golgi marker, but not with the Na^+/K^+ ATPase, a PM marker (Fig. 2F).

Y348D NIS is not only retained intracellularly but also intrinsically inactive

To determine whether the intracellularly retained Y348D NIS mutant is intrinsically active, we investigated I^- transport in MVs prepared from WT or Y348D NIS-expressing Cos-7 cells, enabling us to gain access to NIS molecules in intracellular compartments. As expected (16,20,24), WT NIS-expressing cells transported I^- avidly (Supplementary Fig. S2), and MVs prepared from these cells transported I^- in a Na^+-dependent manner (Fig. 2G). In stark contrast, MVs derived from cells expressing Y348D NIS transported no I^-, demonstrating that Asp at position 348 renders NIS intrinsically inactive.

Hydrophilic residues at position 348 also impair NIS targeting to the cell surface

Cells expressing either Y348H or Y348Q NIS exhibited no ClO_4^--sensitive I^- transport at 10 μM I^- or at 100 μM I^-

FIG. 2. Y348D NIS fails to mature fully and is retained intracellularly. Immunoblot analysis of membrane proteins (10 μg) extracted from MDCK II cells transfected with WT or Y348D NIS cDNA and treated with (+) or without (–) Endo H (**A**) or PNGase-F (**B**). NIS protein forms were detected using an affinity-purified anti-hNIS antibody against residues 618–633 of the carboxy terminus of hNIS. Letters to the right of the blots indicate differently glycosylated states of NIS with different relative electrophoretic mobilities (A: ~90 kDa: mature NIS protein; B, B′: ~60 and ~120 kDa: core glycosylated NIS and its dimer, respectively; C, C′: ~50 and ~100 kDa: deglycosylated NIS and its dimer, respectively). E-cadherin was used as a loading control. (**C**) Flow cytometry analysis (FACS) using an anti-HA antibody to detect total NIS expression (permeabilized cells) or exclusively at the cell surface (nonpermeabilized cells) in MDCK II cells. (**D**) Cell surface biotinylation reveals fully glycosylated WT NIS (**A**) but not Y348D NIS at the PM of MDCK II cells. NIS was detected by immunoblot using the same anti-NIS antibody as in panels (**A, B**). The alpha subunit of the Na^+/K^+ ATPase was used as a loading control. (**E**) Immunofluorescence reveals WT but not Y348D NIS at the PM in nonpermeabilized cells, indicated by colocalization with the Na^+/K^+ ATPase (merge). (**F**) Immunofluorescence under permeabilized conditions shows WT NIS at the PM and expressed intracellularly. Y348D NIS is retained intracellularly. Nonpermeabilized and permeabilized WT and Y348D NIS-transfected MDCK II cells were immunostained with an anti-HA, an anti-Na^+/K^+-ATPase, and an anti-GM130 antibody, followed by anti-rabbit Alexa 488 and anti-mouse Alexa 594-conjugated antibodies. The overlay of the two images is shown (merge). Scale bar = 10 μm. (**G**) I^- transport assays in MVs from control, WT, and Y348D NIS-transduced COS-7 cells carried out at 20 μM I^- in the presence or absence of 100 mM Na^+ for the periods of time indicated (100 μg of protein for each time point). Navy blue (WT, $+Na^+$), pink (WT, $-Na^+$), cyan (Y348D, $+Na^+$), red (Y348D, $-Na^+$), yellow (control). Error bars indicate SE for triplicate determination. COS-7, African green monkey kidney fibroblast-like cell line 7; Endo H, endoglycosidase H; FC, flow cytometry; GM130, Golgi matrix protein 130; MVs, membrane vesicles; PM, plasma membrane; SE, standard error; hNIS, human NIS.

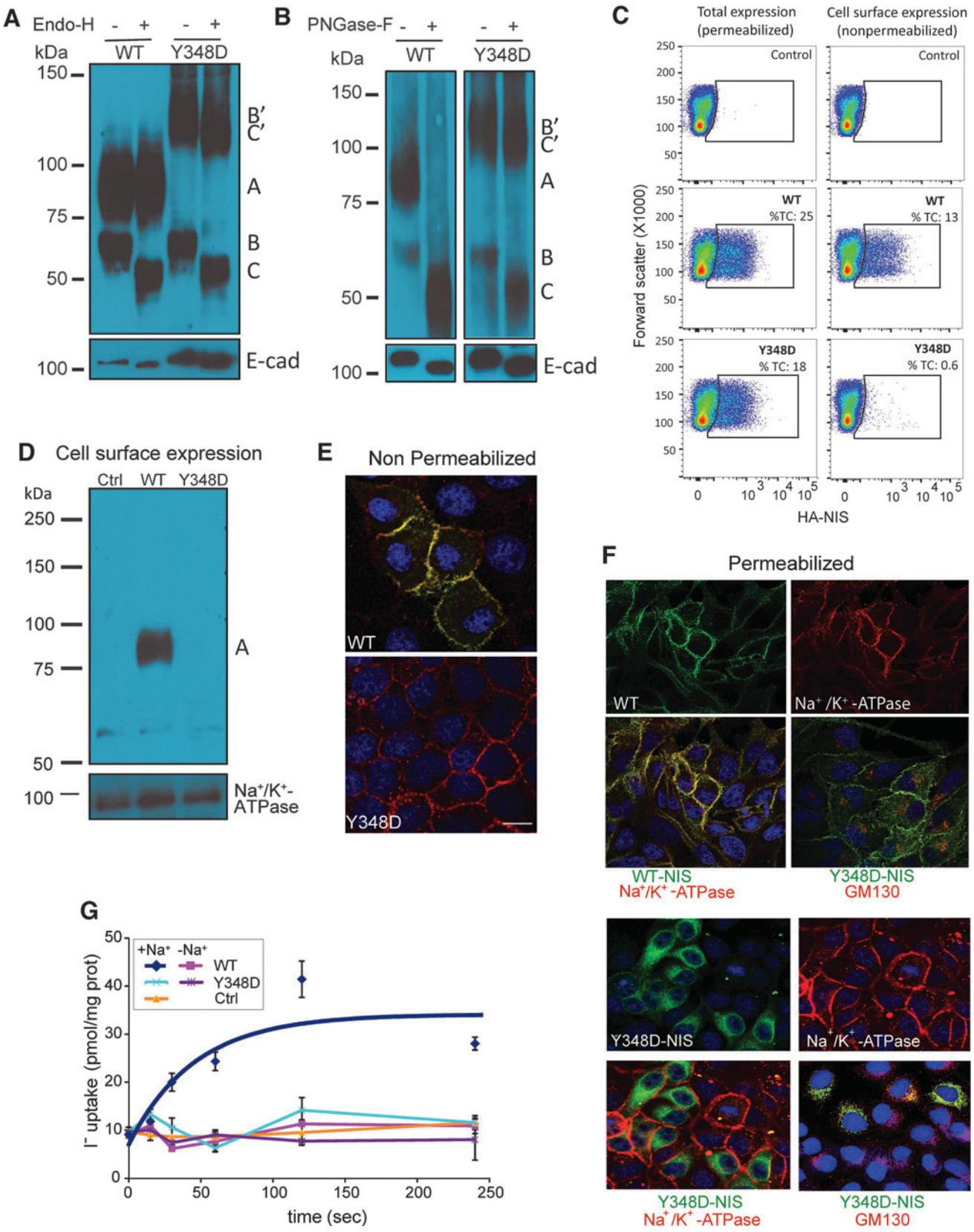
A
Endo-H - + - +
kDa
WT
Y348D
150
100
75
50
100
B′
C′
A
B
C
E-cad
B
PNGase-F - + - +
kDa
WT
Y348D
150
100
75
50
100
B′
C′
A
B
C
E-cad
C
Total expression (permeabilized)
Cell surface expression (nonpermeabilized)
Control
Control
WT
%TC: 25
WT
% TC: 13
Y348D
% TC: 18
Y348D
% TC: 0.6
Forward scatter (X1000)
HA-NIS
D
Cell surface expression
Ctrl WT Y348D
kDa
250
150
100
75
50
100
A
Na+/K+-ATPase
E
Non Permeabilized
WT
Y348D
F
Permeabilized
WT
Na+ /K+ -ATPase
WT-NIS
Na+/K+ -ATPase
Y348D-NIS
GM130
Y348D-NIS
Na+ /K+ -ATPase
Y348D-NIS
Na+ /K+ -ATPase
Y348D-NIS
GM130
G
+Na+ -Na+
WT
Y348D
Ctrl
I- uptake (pmol/mg prot)
time (sec)

(Fig. 3A). FACS (Fig. 3B) and Endo H-plus-Western blot (Fig. 3C) analyses strongly suggest that the defect in Y348Q and Y348H NIS (like that in Y348D NIS) is due to faulty protein processing—specifically, to incomplete glycosylation and impaired delivery to the cell surface. However, when the Western blot for Y348Q and Y348H NIS was overexposed, mature NIS was detected in Y348H NIS-expressing cells, although at very low levels (A ~100 kDa in Supplementary Fig. S3A).

Hydrophobic residues at position 348 rescue NIS targeting to the PM and NIS activity

Given that Y348 is located in a hydrophobic region of NIS (Figs. 1F and 4A), we engineered three hydrophobic residues at position 348—yielding Y348A, Y348L, and Y348F NIS—to ascertain whether they would rescue NIS activity. Indeed, these mutant proteins transported I^- at significant levels, and Y348F NIS, in particular, transported I^- virtually to the same

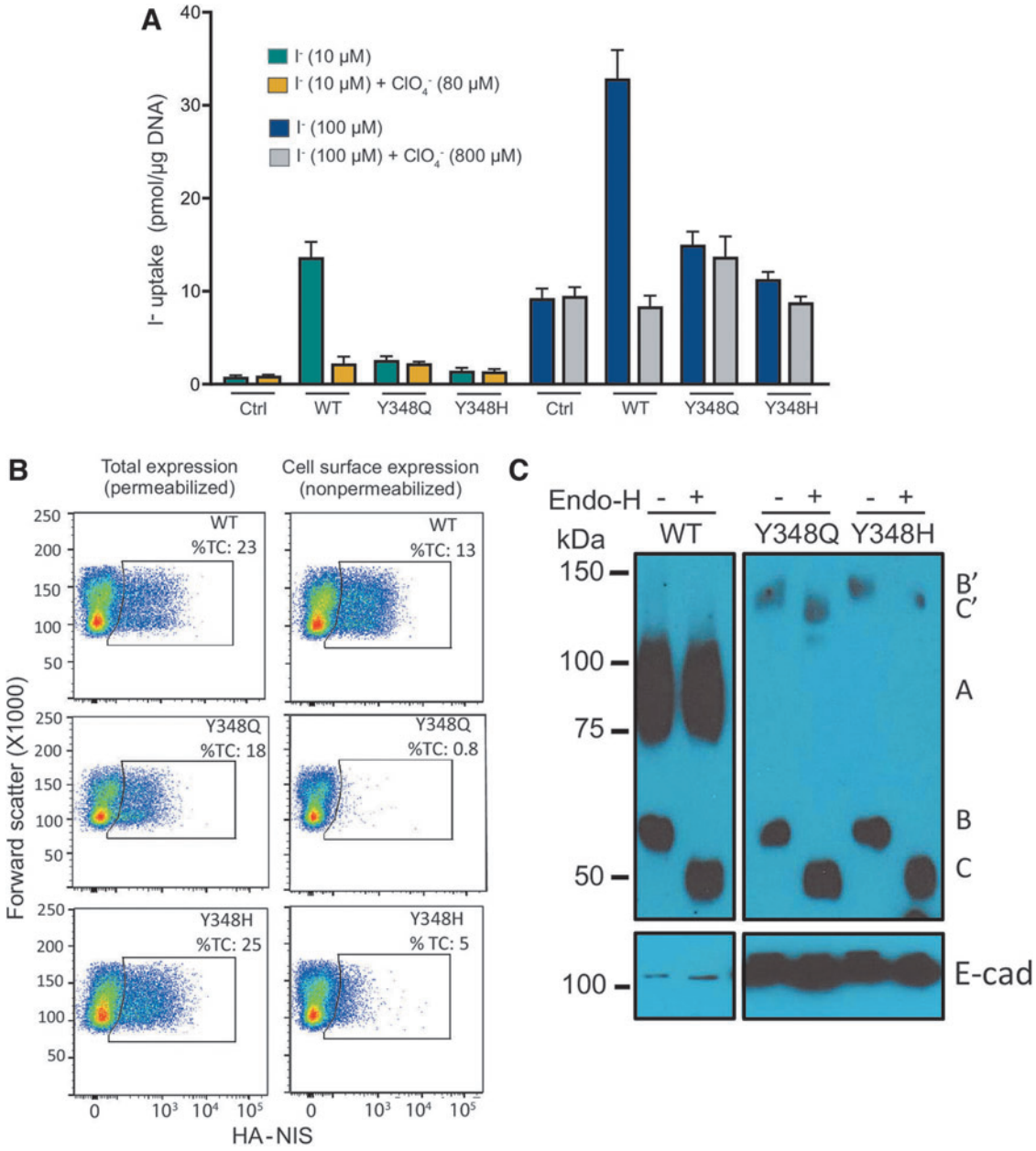

FIG. 3. Hydrophilic amino acids at position 348 render NIS inactive. MDCK-II cells were transfected with control (pcDNA3.1) WT, Y348H, or Y348Q NIS cDNAs. (**A**) Steady-state I^- transport assay (30 min) carried out in the absence (blue bars) or presence (gray bars) of ClO_4^- at 10 μM or 100 μM I^-/140 mM Na^+. Error bars indicate SE for four independent experiments. (**B**) Flow cytometry analysis (FACS) using an anti-HA antibody to detect NIS expression in MDCK-II cells at the cell surface (nonpermeabilized) or anywhere within the cell (permeabilized). (**C**) Immunoblot analysis of membrane proteins (10 μg) obtained from MDCK-II cells transfected with WT, Y348H, or Y348Q NIS, treated with (+) or without (–) Endo H. Letters to the right indicate the relative electrophoretic mobility of the NIS molecules, which depends on the glycosylation of the proteins, as in Figure 2.

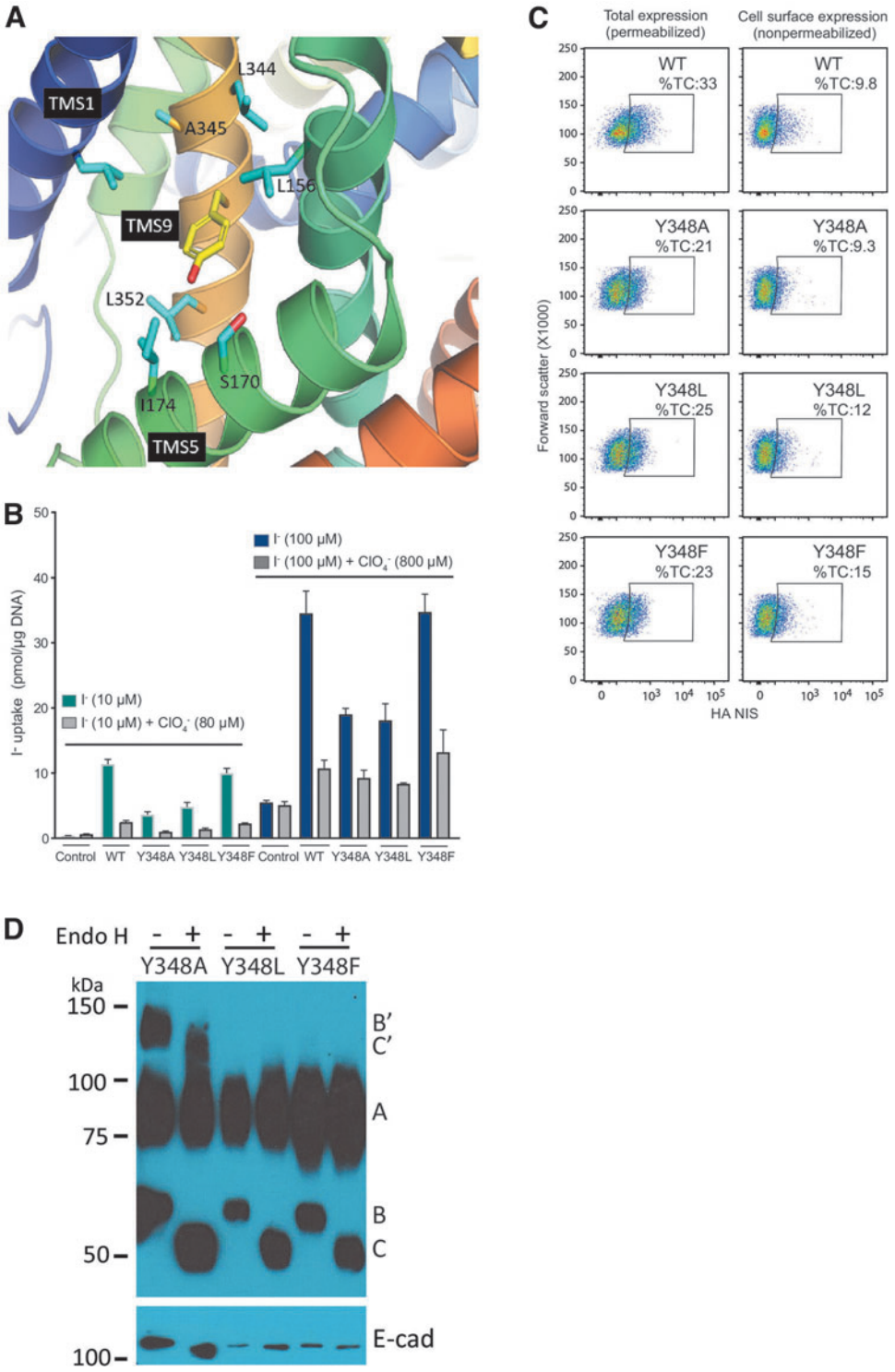

FIG. 4. Hydrophobic residues at position 348 yield active NIS proteins. (**A**) Localization of Y348D in TMS9 and residues in TMS1 (L24), TMS5 (L156, S170, and I174), and TMS9 (L344, A345, and L352) that may interact with Y348D. (**B**) Steady-state I^- transport assay (30 min) in control, WT, Y348A, Y348L, and Y348F NIS-transfected MDCK II cells in the absence (blue bars) or presence (gray bars) of ClO_4^- at 10 μM or 100 μM I^- and 140 mM Na^+. (**C**) Flow cytometry analysis of total expression and cell surface expression of NIS mutants, carried out as in the experiment whose results are shown in Figure 3B. (**D**) Immunoblot analysis of membrane proteins (10 μg) obtained from MDCK-II cells transfected with Y348A, Y348L, or Y348F NIS and treated with (+) or without (−) Endo H. Letters to the right indicate the relative electrophoretic mobility of the NIS molecules, which depends on the glycosylation of the proteins (cf. Fig. 2).

extent as WT NIS (Fig. 4B). As expected, all three proteins reach the PM (Fig. 4C), and they are fully glycosylated (Fig. 4D), just like WT NIS (Fig. 3C). Taken together, these results demonstrate that a hydrophobic residue at position 348 is necessary for proper folding of NIS and for its expression at the PM and that an aromatic ring side chain at this position is required for optimal activity.

The requirement of a hydrophobic residue at position 348 is not due to the interaction of the phenolic ring of Y348 with the membrane fatty acids. Our MD simulations of WT NIS demonstrate that Y348 interacts primarily with hydrophobic residues (i.e., residues side chain non-hydrogen atoms are 5 Å or less from the Y348 side chain). In inwardly open NIS, the side chains of residues L24, L156, L344, A345, L352, and I174 (Fig. 4A) were found to interact with the side chain of Y348 (frequencies: 99.79%, 99.75%, 97.40%, 95.80%, 85.91%, and 98.53%, respectively). In outwardly open NIS, the frequencies were 96.83%, 25.40%, 90.40%, 96.66%, 99.42%, and 15.50%, respectively. Other hydrophobic residues whose side chains frequently interact with Y348 in both

inwardly and outwardly open NIS include F20 (99.34%, 99.66%) and P152 (99.62%, 98.08%). These findings together with the evidence that the Y348F mutation rescues NIS activity to near-WT levels, whereas hydrophilic mutations abrogate I^- transport, support the notion that the hydrophobic environment surrounding residue 348 is an important determinant of NIS stability and function.

Discussion

The ITD-causing mutation Y348D NIS was first identified in three Sudanese patients, one of whom developed a cognitive impairment because she was diagnosed and treated too late (at 40 days of age), whereas her younger siblings, who were diagnosed and treated earlier (at 8 and 22 days of age), developed normally (10). In this study, we report on the molecular characterization of the Y348D NIS mutant and on the requirements at position 348 for NIS function and for the targeting of NIS to the PM.

Although Y348D NIS-expressing cells transported no I^-, even at extremely high concentrations of I^- (10 times the K_M of hNIS) (Fig. 1G and Supplementary Fig. S1), it remained to be determined whether the lack of transport resulted from impaired trafficking of the mutant protein to the PM, impaired intrinsic activity, or both. We demonstrated by glycosidase treatment plus Western blot, FACS, cell surface biotinylation, and immunofluorescence analyses that Y348D NIS is retained intracellularly and that its trafficking to the PM is impaired at or before the *medial*-Golgi (Fig. 2A–F).

Defects in the biosynthesis of PM proteins that prevent them from being trafficked to the cell surface have been shown to cause loss of function in several other membrane transporters belonging to the Slc5 family (39–42). In our study, we found that Y348D NIS is only partially glycosylated. However, this alone may not account for the protein's intracellular retention and loss of activity since non-glycosylated NIS is targeted to the PM and has kinetic parameters very similar to those of WT NIS (5,24). Instead, it is likely that Y348D NIS is retained intracellularly because it is improperly folded—although, if so, nothing can be concluded from this about the protein's intrinsic activity.

Some ITD-causing NIS mutants are retained intracellularly either partially or completely but are nonetheless intrinsically active (16,26); by contrast, some other mutants are intracellularly retained and intrinsically inactive (20,24). MVs prepared from cells expressing Y348D NIS transported no I^-, demonstrating that this NIS mutant, in addition to being retained intracellularly, is also intrinsically inactive (Fig. 2G).

Not all ITD-causing NIS mutants are retained intracellularly. Indeed, several mutants are trafficked to the PM but intrinsically nonfunctional (17,18,23). One of these—T354P NIS—was the very first ITD-causing NIS mutant identified in a patient (14,17), and the investigation of the molecular requirements of NIS at position 354 has yielded a great deal of valuable mechanistic information (21). Ultimately, on the basis of experiments guided by MD simulations informed by our NIS homology model, we reported that, in addition to S353 and T354, four other residues—S66, D191, Q194, and Q263—participate in Na^+ coordination at the Na2 binding site (21,27).

According to our NIS homology model, although Y348 is also located in TMS9, it does not face the Na^+ translocation pathway. Instead, Y348 is on the opposite side of the helix, where it is surrounded mostly by hydrophobic residues (Fig. 1D–F). Because TMS9 is tilted with respect to the plane of the membrane, the residue at position 348 is in contact with several other residues, which contribute to maintaining its geometric relation to the TMSs perpendicular to the membrane. Consistent with this notion, NIS proteins with hydrophobic residues at position 348 are properly trafficked to the PM, and they partially or fully retain transport activity (Fig. 4B). In contrast, the presence of Asp, a negatively charged residue, at position 348 may prevent TMS9 from being properly inserted into the membrane during NIS biosynthesis, thus destabilizing the folding of the protein and interfering with its activity (Fig. 1G). This idea is supported by our finding that other hydrophilic residues at position 348 also impair NIS trafficking to the PM and NIS-mediated I^- transport (Fig. 3A–C).

A homology model of hNIS was recently proposed by Zhekova *et al*. (43). Although their article describes an extensive procedure involving multiple sequence alignment and threading with several structural templates, the final NIS model they used for refinement and MD simulations was based on the structure of vSGLT, the same structural template that we used to generate the model we have published (16,23,24,26) and that we used in this work for the inwardly open NIS. Although Zhekova *et al.* did not present a model of outwardly open NIS, they mentioned the outward-facing structure of SiaT when describing the putative mechanism associated with the transition between the outwardly and inwardly facing conformations of NIS. Our model and MD simulations of outwardly open NIS are based on the structure of SiaT. Overall, the predictions emerging from our homology models and MD simulations are consistent with all published experimental data on NIS.

A phylogenetic analysis of the SLC5 family demonstrates that a hydrophobic residue at the position corresponding to NIS-348 is highly conserved across all members of the family (Supplementary Figs. S4 and S5).

ITD must be detected by early neonatal screening to ensure that the condition can be treated with THs before it causes permanent cognitive and developmental deficits. I^- supplementation during pregnancy is also beneficial, especially in countries where I^- deficiency is still prevalent. ClO_4^- pollution in water sources should also be taken into consideration.

We have demonstrated that ClO_4^- is not only transported by NIS as a substrate (37) but also that ClO_4^- allosterically prevents Na^+ from binding to one of its binding sites (44). This has a profound effect on the mechanism by which NIS transports I^-: ClO_4^- changes the stoichiometry of I^- transport from electrogenic (2 Na^+:1 I^-) to electroneutral (1 Na^+:1 I^-), markedly decreasing I^- transport in the thyroid, and consequently reducing biosynthesis of the THs (44). Thus, exposure to high concentrations of ClO_4^- may be more deleterious than previously thought, particularly to pregnant and nursing women and their fetuses and newborns.

Our findings indicate that Y348 plays a significant role in both the activity of NIS and its targeting to the PM, demonstrating that a single amino acid mutation in a key protein can have severe health effects that can last a lifetime. It is imperative that the thyroid status of all newborns be monitored so that, when early interventions are necessary, they can be carried out immediately, before the newborns suffer irreversible cognitive damage.

Acknowledgments

We thank the members of the Carrasco Laboratory and Dr. Biff Forbush for their insightful comments and for helpful discussion.

Authors' Contributions

A.R-N., L.J., and N.C. designed the research. A.R-N., L.J., M.X.S., and M.C. performed the research. A.R-N., L.J., M.C., L.M.A., and N.C. analyzed the data. A.R-N, M.C, L.M.A., and N.C. wrote the article.

Author Disclosure Statement

No competing financial interests exist.

Funding Information

This work was supported by the National Institutes of Health (NIH) GM-114250 (to N.C. and L.M.A.). A.R.-N. was supported in part by ATA R13153. L.J. was supported by the German Academy Foundation Scholarship. M.X.S. was supported by the Queen's University Belfast Fellowship. This work was made possible in part by the computational resources and scientific computing services at the Maryland Advanced Research Computing Center (MARCC).

Supplementary Material

Supplementary Figure S1
Supplementary Figure S2
Supplementary Figure S3
Supplementary Figure S4
Supplementary Figure S5

References

1. Zimmermann MB, Boelaert K 2015 Iodine deficiency and thyroid disorders. Lancet Diabetes Endocrinol **3:**286–295.
2. The Iodine Global Network 2020 Global Scorecard of Iodine Nutrition in 2020 in the General Population Based on School-Age Children (SAC). IGN, Ottawa, Canada.
3. Carrasco N 1993 Iodide transport in the thyroid gland. Biochim Biophys Acta **1154:**65–82.
4. Dai G, Levy O, Carrasco N 1996 Cloning and characterization of the thyroid iodide transporter. Nature **379:** 458–460.
5. Levy O, De la Vieja A, Ginter CS, Riedel C, Dai G, Carrasco N 1998 N-linked glycosylation of the thyroid Na^+/I^- symporter (NIS). Implications for its secondary structure model. J Biol Chem **273:**22657–22663.
6. Eskandari S, Loo DD, Dai G, Levy O, Wright EM, Carrasco N 1997 Thyroid Na+/I- symporter. Mechanism, stoichiometry, and specificity. J Biol Chem **272:**27230–27238.
7. Nicola JP, Carrasco N, Mario Amzel L 2014 Physiological sodium concentrations enhance the iodide affinity of the Na^+/I^- symporter. Nat Commun **5:**3948.
8. Ravera S, Reyna-Neyra A, Ferrandino G, Amzel LM, Carrasco N 2017 The sodium/iodide symporter (NIS): molecular physiology and preclinical and clinical applications. Annu Rev Physiol **79:**261–289.
9. Martin M, Modenutti CP, Geysels RC, Peyret V, Signorino M, Testa G, Masini-Repiso AM, Miras M, Carrasco N, Marti MA, Nicola JP 2018 A novel iodide transport defect-causing Na^+/I^- symproter (NIS) carboxy-terminus mutant uncovers a critical trypthophan-acid motif required for plasma membrane transport. Thyroid **28:**A-3 (Abstract).
10. Watanabe Y, Ebrhim RS, Abdullah MA, Weiss RE 2018 A novel missense mutation in the SLC5A5 gene in a sudanese family with congenital hypothyroidism. Thyroid **28:**1068–1070.
11. Stoupa A, Al Hage Chehade G, Kariyawasam D, Tohier C, Bole-Feysot C, Nitschke P, Thibault H, Jullie ML, Polak M, Carre A 2020 First case of fetal goitrous hypothyroidism due to SLC5A5/NIS mutations. Eur J Endocrinol **183:**K1–K5.
12. Kosugi S, Inoue S, Matsuda A, Jhiang SM 1998 Novel, missense and loss-of-function mutations in the sodium/iodide symporter gene causing iodide transport defect in three Japanese patients. J Clin Endocrinol Metab **83:**3373–3376.
13. Fujiwara H, Tatsumi K, Tanaka S, Kimura M, Nose O, Amino N 2000 A novel V59E missense mutation in the sodium iodide symporter gene in a family with iodide transport defect. Thyroid **10:**471–474.
14. Fujiwara H 1997 Congenital hypothyroidism caused by a mutation in the Na+/l-symporter. Nat Genet **17:**122.
15. Martin M, Bernal Barquero CE, Geysels RC, Papendieck P, Peyret V, Masini-Repiso AM, Chiesa AE, Nicola JP 2019 Novel sodium/iodide symporter compound heterozygous pathogenic variants causing dyshormonogenic congenital hypothyroidism. Thyroid **29:**1023–1026.
16. Nicola JP, Reyna-Neyra A, Saenger P, Rodriguez-Buritica DF, Godoy JD, Muzumdar R, Amzel LM, Carrasco N 2015 The sodium/iodide symporter mutant V270E causes stunted growth but no cognitive deficiency. J Clin Endocrinol Metab **100:**E1353–E1361.
17. Levy O, Ginter CS, De la Vieja A, Levy D, Carrasco N 1998 Identification of a structural requirement for thyroid Na^+/I^- symporter (NIS) function from analysis of a mutation that causes human congenital hypothyroidism. FEBS Lett **429:**36–40.
18. Dohan O, Gavrielides MV, Ginter C, Amzel LM, Carrasco N 2002 Na^+/I^- symporter activity requires a small and uncharged amino acid residue at position 395. Mol Endocrinol **16:**1893–1902.
19. De La Vieja A, Ginter CS, Carrasco N 2004 The Q267E mutation in the sodium/iodide symporter (NIS) causes congenital iodide transport defect (ITD) by decreasing the NIS turnover number. J Cell Sci **117:**677–687.
20. De la Vieja A, Ginter CS, Carrasco N 2005 Molecular analysis of a congenital iodide transport defect: G543E impairs maturation and trafficking of the Na^+/I^- symporter. Mol Endocrinol **19:**2847–2858.
21. De la Vieja A, Reed MD, Ginter CS, Carrasco N 2007 Amino acid residues in transmembrane segment IX of the Na^+/I^- symporter play a role in its Na+ dependence and are critical for transport activity. J Biol Chem **282:**25290–25298.
22. Reed-Tsur MD, De la Vieja A, Ginter CS, Carrasco N 2008 Molecular characterization of V59E NIS, a Na^+/I^- symporter (NIS) mutant that causes congenital I- transport defect (ITD). Endocrinology **149:**3077–3084.
23. Paroder-Belenitsky M, Maestas MJ, Dohan O, Nicola JP, Reyna-Neyra A, Follenzi A, Dadachova E, Eskandari S, Amzel LM, Carrasco N 2011 Mechanism of anion selectivity and stoichiometry of the Na^+/I^- symporter (NIS). Proc Natl Acad Sci U S A **108:**17933–17938.

24. Li W, Nicola JP, Amzel LM, Carrasco N 2013 Asn441 plays a key role in folding and function of the Na^+/I^- symporter (NIS). FASEB J **27:**3229–3238.
25. Jung L, Reyna MA, Suarez MX, Carrasco N 2018 Molecular characterization of a novel mutant NIS protein found in a patient with congenital hypothyroidism. Thyroid **28:** 182 (Abstract).
26. Paroder V, Nicola JP, Ginter CS, Carrasco N 2013 The iodide transport defect-causing mutation R124H: a delta-amino group at position 124 is critical for maturation and trafficking of the Na^+/I^- symporter (NIS). J Cell Sci **126:** 3305–3313.
27. Ferrandino G, Nicola JP, Sanchez YE, Echeverria I, Liu Y, Amzel LM, Carrasco N 2016 Na^+ coordination at the Na2 site of the Na^+/I^- symporter. Proc Natl Acad Sci U S A **113:** E5379–E5388.
28. Faham S, Watanabe A, Besserer GM, Cascio D, Specht A, Hirayama BA, Wright EM, Abramson J 2008 The crystal structure of a sodium galactose transporter reveals mechanistic insights into Na+/sugar symport. Science **321:**810–814.
29. Watanabe A, Choe S, Chaptal V, Rosenberg JM, Wright EM, Grabe M, Abramson J 2010 The mechanism of sodium and substrate release from the binding pocket of vSGLT. Nature **468:**988–991.
30. Wahlgren WY, Dunevall E, North RA, Paz A, Scalise M, Bisignano P, Bengtsson-Palme J, Goyal P, Claesson E, Caing-Carlsson R, Andersson R, Beis K, Nilsson UJ, Farewell A, Pochini L, Indiveri C, Grabe M, Dobson RCJ, Abramson J, Ramaswamy S, Friemann R 2018 Substrate-bound outward-open structure of a Na(+)-coupled sialic acid symporter reveals a new Na(+) site. Nat Commun **9:**1753.
31. Van Der Spoel D, Lindahl E, Hess B, Groenhof G, Mark AE, Berendsen HJ 2005 GROMACS: fast, flexible, and free. J Comput Chem **26:**1701–1718.
32. Abraham MJ MT, Schulz R, Pall S, Smith JC, Hess B, Lindahl E. 2015 GROMACS: high performance molecular simulations through multi-level parallelism from laptops to supercomputers. SoftwareX **1–2:**19–25.
33. Klauda JB, Venable RM, Freites JA, O'Connor JW, Tobias DJ, Mondragon-Ramirez C, Vorobyov I, MacKerell AD, Jr, Pastor RW 2010 Update of the CHARMM all-atom additive force field for lipids: validation on six lipid types. J Phys Chem B **114:**7830–7843.
34. Jo S, Kim T, Iyer VG, Im W 2008 CHARMM-GUI: a web-based graphical user interface for CHARMM. J Comput Chem **29:**1859–1865.
35. Wu EL, Cheng X, Jo S, Rui H, Song KC, Davila-Contreras EM, Qi Y, Lee J, Monje-Galvan V, Venable RM, Klauda JB, Im W 2014 CHARMM-GUI Membrane Builder toward realistic biological membrane simulations. J Comput Chem **35:**1997–2004.
36. Lee J CX, Swails JM, Yeom MS, Eastman PK, Lemkul JA, Wei S, Buckner J, Jeong JC, Qi Y, Jo S, Pande VS, Case DA, Brooks CL, MacKerell AD, Klauda JB, Im W. 2016 CHARMM-GUI Input Generator for NAMD, GROMACS, AMBER, OpenMM, and CHARMM/OpenMM Simulations using the CHARMM36 Additive Force Field. J Chem Theory Comput **12:**405–413.
37. Dohan O, Portulano C, Basquin C, Reyna-Neyra A, Amzel LM, Carrasco N 2007 The Na^+/I^- symporter (NIS) mediates electroneutral active transport of the environmental pollutant perchlorate. Proc Natl Acad Sci U S A **104:**20250–20255.
38. Tazebay UH, Wapnir IL, Levy O, Dohan O, Zuckier LS, Zhao QH, Deng HF, Amenta PS, Fineberg S, Pestell RG, Carrasco N 2000 The mammary gland iodide transporter is expressed during lactation and in breast cancer. Nat Med **6:** 871–878.
39. Schumann T, Konig J, Henke C, Willmes DM, Bornstein SR, Jordan J, Fromm MF, Birkenfeld AL 2020 Solute carrier transporters as potential targets for the treatment of metabolic disease. Pharmacol Rev **72:**343–379.
40. Martin MG, Turk E, Lostao MP, Kerner C, Wright EM 1996 Defects in Na+/glucose cotransporter (SGLT1) trafficking and function cause glucose-galactose malabsorption. Nat Genet **12:**216–220.
41. Subramanian VS, Constantinescu AR, Benke PJ, Said HM 2017 Mutations in SLC5A6 associated with brain, immune, bone, and intestinal dysfunction in a young child. Hum Genet **136:**253–261.
42. Byrne AB, Arts P, Polyak SW, Feng J, Schreiber AW, Kassahn KS, Hahn CN, Mordaunt DA, Fletcher JM, Lipsett J, Bratkovic D, Booker GW, Smith NJ, Scott HS 2019 Identification and targeted management of a neurodegenerative disorder caused by biallelic mutations in SLC5A6. NPJ Genom Med **4:**28.
43. Zhekova HR, Sakuma T, Johnson R, Concilio SC, Lech PJ, Zdravkovic I, Damergi M, Suksanpaisan L, Peng KW, Russell SJ, Noskov S 2020 Mapping of ion and substrate binding sites in human sodium iodide symporter (hNIS). J Chem Inf Model **60:**1652–1665.
44. Llorente-Esteban A, Manville RW, Reyna-Neyra A, Abbott GW, Amzel LM, Carrasco N 2020 Allosteric regulation of mammalian Na^+/I^- symporter activity by perchlorate. Nat Struct Mol Biol **27:**533–539.

Address correspondence to:
Nancy Carrasco, MD
Department of Molecular Physiology and Biophysics
Vanderbilt University School of Medicine
2215 Garland Avenue, 707 Light Hall
Nashville, TN 37232-0615
USA

E-mail: nancy.carrasco@vanderbilt.edu